Available online at www.sciencedirect.com
ScienceDirect
Advances in Space Research 71 (2023) 4604–4612
ADVANCES IN SPACE RESEARCH
(a COSPAR publication)
www.elsevier.com/locate/asr

Ion acoustic waves in lunar wake plasma ☆

T. Sreeraj *, S.V. Singh, G.S. Lakhina

Indian Institute of Geomagnetism, New Panvel (W), Navi Mumbai 410218, India

Received 22 August 2022; received in revised form 9 January 2023; accepted 13 January 2023
Available online 21 January 2023

Abstract

Kinetic theory of low frequency electrostatic waves is carried out in the lunar wake plasma modelled by kappa electrons, kappa-beam electrons, Maxwell–Boltzmann distributed protons and doubly charged Helium ions. The present work is motivated by observation of electrostatic waves on the outbound side of the first lunar wake flyby of the mission Acceleration, Reconnection, Turbulence and Electrodynamics of the Moon's Interaction with the Sun (ARTEMIS) probe P1. The dispersion characteristics of electrostatic waves which are identified as ion-acoustic waves are carried out for the observational plasma parameters. The frequencies of the ion acoustic waves derived from the model corresponding to peak growth rates are $f \leqslant 0.02 f_{pe}$; (f_{pe} being electron plasma frequency) which matches with the frequency of the waves observed by wave burst 1 (WB1) in the lunar wake (Tao et al., 2012). Our theoretical analysis reveals that in order to excite the low-frequency wave modes, low-energy electron beams are required which are not apparent in the observations.

Keywords: Electrostatic wave; Kinetic theory; Lunar wake; Solar wind

1. Introduction

When an object intercepts the fluid flow, the region formed behind that object is called as wake region. The streaming solar wind is blocked by the moon and hence lunar wake region is formed behind the moon (Bosqued et al., 1996). The plasma density in the immediate downstream of the wake region is highly depleted in comparison with those outside the wake (Hutchinson and Malaspina, 2018). Recent study undertaken by Guo et al. (2019) has shown a significant depression in magnetic field caused by the refilling of dense plasma clouds (with densities of 0.20–0.47 cm^{-3}) into the near lunar wake. There have been several studies to understand various plasma processes in this region [see Bhardwaj et al. (2015) and references therein.].

Ion acoustic waves (IAW) are one of the fundamental modes that exist in unmagnetized plasma. The pioneering work was conducted by Fried (1961) in a two-component plasma comprising of electron and ions, where it was shown that these oscillations are highly damped unless temperature of electrons becomes much higher than that of ions. Wong et al. (1964) were the first to verify the existence of IAWs in laboratory plasmas. IAWs have been observed in various plasma environments, e.g., laboratory plasmas (Lonngren et al., 1967), in the interplanetery shocks (Hess et al., 1998), auroral magnetic field lines (Backrud et al., 2005), solar wind (Forslund, 1970), cometary environment(Scarf et al., 1986) and in lunar wake (Bale, 1997; Bale et al., 1997). In addition to IAWs, a wide variety of plasma waves are observed near the Moon (for a comprehensive review, please refer Harada and Halekas (2016), Nakagawa (2016)).

Most of the space plasmas are characterized by the particle distributions that are having energetic tails and cannot be modeled by classic Maxwell–Boltzmann distribution function. Instead, these are modelled by generalized

☆IAW in lunar wake plasma.
* Corresponding author.
E-mail address: sreerajt90@gmail.com (T. Sreeraj).

https://doi.org/10.1016/j.asr.2023.01.034
0273-1177/

Lorentzian distribution or kappa distribution function and were first encountered by Olbert (1968) when analyzing the data from IMP-1 satellite. Later on, it was used by Vasyliunas (1968) to fit the electron number density data in the magnetosphere by Orbiting Geophysical Observatory 1 (OGO 1) and OGO 3 satellite. Thereafter, kappa distributions have been often observed in space plasmas [for an extensive review, see Livadiotis (2015) and references therein]. The kappa distributions have also been observed in lunar wake (Halekas, 2005).

An extensive study was carried out by Meng et al. (1992) in an unmagnetized plasma comprising of drifting electrons and protons modeled by kappa distribution. It was shown that for a highly nonthermal plasma, the critical speeds required to excite the instability are smaller compared to the Maxwell–Boltzmann plasma, provided ions are relatively cold. A larger drift velocity is required, when the ions become warm. When ions becomes much hotter kappa distribution makes the system more unstable. Summers and Thorne (1992) studied the ion acoustic waves in two component plasma comprising of drifting kappa electrons and kappa ions. They have shown that ion acoustic waves get highly damped with increase in superthermality index. Further, for sufficiently large drift speed, ion acoustic waves are destabilized at larger wavelengths. Effect of superthermality index and other plasma parameters on growth of IAWs have also been studied in dusty and cometary plasmas (Zaheer et al., 2004; Liu and Du, 2009; ur Rehman et al., 2019; Chen et al., 2019).

A comprehensive study conducted by Tao et al. (2012) using Acceleration, Reconnection, Turbulence and Electrodynamics of the Moon's Interaction with the Sun (ARTEMIS) P1 spacecraft data has shown the existence of electrostatic waves in the lunar wake. ARTEMIS mission is derived from Time History of Events and Macroscale Interactions during Substorms (THEMIS) mission, which comprised of 5 satellites named from A to E. THEMIS-B and THEMIS-C, were re-positioned to approach moon and subsequently renamed as ARTEMIS-P1 and ARTEMIS-P2, respectively (Angelopoulos, 2008). During this process, they performed flybys through lunar wake. Lunar wake crossing which happened on 13-February-2010 was the subject of extensive study undertaken by Tao et al. (2012). The plasma environment in the lunar wake is summarised in Fig. 1. Vertical black dashed lines indicates the time in which ARTEMIS P1 was in lunar wake. Fig. 1a represents the ion density. Fig. 1b shows the ion flow velocity in solar wind in SSE coordinates (Selenocentric Solar Ecliptic) coordinates. This remained approximately constant throughout the flyby. Temperature of electron (with it's parallel and perpendicular component) is shown in Fig. 1c, which peaks near to center of lunar wake. The components of magnetic field in SSE coordinates are shown in Fig. 1d. Fig. 1e displays differential energy flux of parallel electrons. Spectrum of electric field from onboard digital field board (DFB) (Cully et al., 2008) shows enhancement during 09:10 to 09:25 UT (Fig. 1f). Magnetic field spectrogram does not show any enhancements, indicating that the observed waves are electrostatic in nature. Particle data is derived from electrostatic analyzer (ESA) (McFadden et al., 2008). Three solid black vertical lines spanning Fig. 1e & f indicate the time at which high resolution electric field burst data are available. These wave bursts are indicated as WB1, WB2 and WB3. Employing the data from the lunar wake crossing in the same time that was mentioned by Tao et al. (2012), Wiehle et al. (2011) has conducted three dimensional hybrid simulation. They have found out that magneto hydrodynamic mode (fast, slow and Alfven modes) are observed in simulated wake. Halekas et al. (2011) analyzed the data from the same time interval and showed that the wake is being refilled by electrons, interpenetrating protons and alpha particles from both the flanks along the magnetic field lines. These creates favorable condition for generation of different electrostatic instabilities.

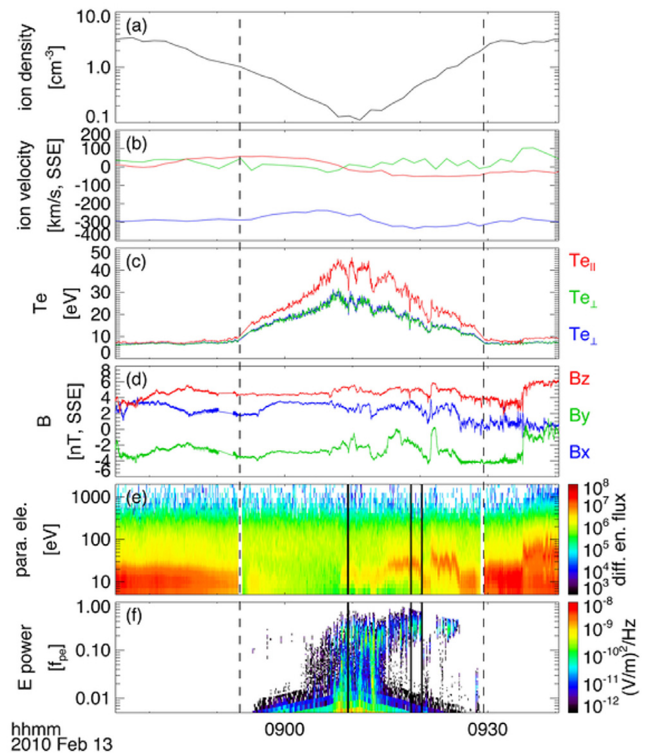

Fig. 1. Various plasma parameters observed by ARTEMIS P1 during the flyby on 2010 Feb 13. Vertical dashed line indicates the time in which the spacecraft moved onto lunar wake. Panel (a) shows ion density, panel (b) shows ion velocity in Selenocentric Solar Ecliptic (SSE) coordinate system, panel (c) shows the electron temperature, with red being the field-aligned temperature and green & blue depicts the perpendicular temperature, panel (d) shows the magnetic field in SSE coordinates, panel (e) displays the differential energy flux of parallel electrons and panel (f) displays electric field power spectrum obtained from onboard digital field board. The frequencies has been normalized with local electron plasma frequency (f_{pe}). The black vertical bar in panel (e) and (f) indicate the time of three wave bursts, i.e. WB1, WB2 and WB3. (Figure reprinted with permission from Tao, J. B. et al. (2012), Kinetic instabilities in the lunar wake: ARTEMIS observations, J. Geophys. Res., 117, A03106, doi:10.1029/2011JA017364).

Using 1-D Vlasov simulation, Tao et al. (2012) showed that the waves with frequencies in the range of $\approx$ (0.1–0.4) f_{pe}, where f_{pe} is the electron plasma frequency, can be generated by the kinetic instabilities of electron beam mode. Thereafter, there has been several attempts to develop theoretical models to explain the wave bursts WB1, WB2 and WB3 observed by ARTEMIS P1 satellite by Tao et al. (2012). Modeling the lunar wake plasma by hot protons, hot heavier ions (α-particles, He^{++}), electron beam and suprathermal electrons following kappa distribution, Rubia et al. (2017) have tried to explain the low frequency part of the spectrum in terms of slow and fast ion acoustic solitons. Based on the fluid model proposed by Rubia et al. (2017), Sreeraj et al. (2018) considered unmangetised lunar wake plasma modeled by proton, doubly charged Helium, beam electron (all three in Maxwell–Boltzmann distribution) and kappa electrons. They have found that as the beam velocity increases, the phase velocity of electron acoustic mode increases from negative to positive. At a certain threshold value of electron beam velocity, the mode which has gained the positive phase speed merges with slow ion acoustic mode and becomes unstable thereby generating positive growth rate. Further, they have carried out extensive parametric studies. The frequency corresponding to maximum growth rate from their model matches with the observation from satellite. Sreeraj et al. (2020) extended the fluid model in Sreeraj et al. (2018) to study the propagation characteristics of low and high frequency electrostatic waves in magnetized plasmas. They found that the various modes couple with each other and could produce non-resonant instability. Though different authors have shown the presence of electrostatic waves in this lunar flyby and also analyzed the waves in the context of fluid theory, nobody has undertaken the study employing kinetic theory to explore the possibility of resonant instability that can be excited in this system. In the present study, we use the kinetic theory to study the excitation of electrostatic waves in the lunar wake which is more in-sync with the 1-D, electrostatic Vlasov simulations conducted by Tao et al. (2012). In this theoretical work, the generation of low-frequency electrostatic waves observed in WB1 by ARTEMIS P1 (Tao et al., 2012) is undertaken. The WB1 has low-frequency component which can reach as low as 0.01f_{pe} which could not be explained by electron beam mode. For the sake of completeness, we allow few percentage of He^{++} ions (which are likely to be present in the lunar wake as discussed by Halekas et al. (2011)) in addition to Maxwellian protons, and two electron components having kappa-distributions.

2. Kinetic plasma model

The lunar wake plasma is modeled by homogeneous, collisionless four-component plasma comprising of background protons (n_{0p}, T_p), doubly charged helium ions, He^{++} (n_{0i}, T_i), background electrons (n_{0e}, T_e) and beam electrons (n_{0b}, T_b, U_b) streaming along ambient magnetic field, $\mathbf{B}_0$ which is considered to be in z direction. The background protons and helium ions follow Maxwellian distribution whereas background electrons and beam electrons are assumed having suprathermal kappa distribution. The suprathermal kappa distribution is given by (Mace and Hellberg, 1995):

$$f_s = \frac{n_{0s}}{(\pi\kappa)^{\frac{3}{2}}\theta_s^3}\frac{\Gamma(\kappa+1)}{\Gamma(\kappa-\frac{1}{2})}\left[1+\frac{(v-U_s)^2}{\kappa\theta_s^2}\right]^{-(\kappa+1)} \quad (1)$$

The subscript $s = e,\ b,\ p,\ i$ stands for kappa background electrons, kappa beam electrons, protons, doubly charged helium ions, respectively. Here, n_{0s}, T_s, U_s are the unperturbed number density, temperature and beam velocity of species 's', κ is the superthermality index, $\theta_s = v_{ts}\sqrt{\frac{2\kappa-3}{2\kappa}}$ is the modified thermal speed and $v_{ts} = \sqrt{\frac{2T_s}{m_s}}$ is the thermal velocity for Maxwellian species, where T_s is in units of energy and m_s is the mass of species 's'. From the expression for modified thermal velocity, it is clear that in order to have a meaningful value for the thermal speed, $\kappa > \frac{3}{2}$. In the limit $\kappa \to \infty$, suprathermal kappa distribution reduces to Maxwellian distribution and is valid for background protons and helium ions considered in the present model.

The plasma dielectric function for electrostatic waves for our model can be written as (Mace and Hellberg, 1995)

$$\begin{aligned} D(\omega,k) = 1 &+ \frac{2\omega_{pe}^2}{k^2\theta_e^2}\left[\frac{2\kappa-1}{2\kappa}+\frac{\omega}{k\theta_e}Z_\kappa\left(\frac{\omega}{k\theta_e}\right)\right] \\ &+ \frac{2\omega_{pb}^2}{k^2\theta_b^2}\left[\frac{2\kappa-1}{2\kappa}+\frac{\omega}{k\theta_b}Z_\kappa\left(\frac{\omega-kU_b}{k\theta_b}\right)\right] \\ &+ \frac{2\omega_{pi}^2}{k^2v_{ti}^2}\left[1+\frac{\omega}{kv_{ti}}Z\left(\frac{\omega}{kv_{ti}}\right)\right] + \frac{2\omega_{pp}^2}{k^2v_{tp}^2}\left[1+\frac{\omega}{kv_{tp}}Z\left(\frac{\omega}{kv_{tp}}\right)\right] \end{aligned} \quad (2)$$

Here, $\theta_e = v_{te}\sqrt{\frac{2\kappa-3}{2\kappa}}$ and $\theta_b = v_{tb}\sqrt{\frac{2\kappa-3}{2\kappa}}$ are modified thermal speed of kappa background electrons and kappa beam electrons; plasma frequency of s^{th} species is given as $\omega_{ps} = \left(\frac{n_{0s}z_s^2e^2}{\epsilon_0 m_s}\right)^{1/2}$, where z_s is the charge number of the species 's'; U_b is the drift velocity of kappa electron beam. For doubly charged helium, $z_i = 2$, and all other species it is unity.

The dispersion relation for electrostatic waves can be obtained by setting $D(\omega,k) = 0$. Further, to obtain analytical expression for dispersion relation, dispersion function Z_κ(Mace and Hellberg, 1995) for both electrons (background and beam electrons) is expanded in small phase velocity limit, i.e., $\frac{\omega}{k\theta_e} \ll 1$ and $\frac{\omega-ku_b}{k\theta_e} \ll 1$, whereas for protons and Helium ions is expanded in large phase velocity limit, i.e., $\frac{\omega}{kv_{tp}} \gg 1$ and $\frac{\omega}{kv_{ti}} \gg 1$. Substituting $\omega = \omega_r + i\gamma, \gamma \ll \omega_r$ in Eq. (2) and separating real and imaginary parts, dispersion relation can be written as

$$D(\omega_r,k) = D_r(\omega,k) + iD_i(\omega,k) = 0 \quad (3)$$

where real part is given by:

$$D_r = 1 + \frac{2\kappa-1}{2\kappa-3}\frac{1}{k^2\lambda_{De}^2} + \frac{2\kappa-1}{2\kappa-3}\frac{1}{k^2\lambda_{Db}^2} - \frac{(4\kappa^2-1)}{(2\kappa-3)^2}\left[\frac{4\omega^2\omega_{pe}^2}{k^4 v_{te}^4} + \frac{4(\omega-kU_b)^2\omega_{pb}^2}{k^4 v_{tb}^4}\right] - \frac{\omega_{pi}^2}{\omega^2}\left[1+\frac{3}{2}\frac{k^2 v_{ti}^2}{\omega^2}\right] - \frac{\omega_{pp}^2}{\omega^2}\left[1+\frac{3}{2}\frac{k^2 v_{tp}^2}{\omega^2}\right] \quad (4)$$

and imaginary part becomes:

$$D_i = \sqrt{\pi}\left[\frac{2\omega_{pe}^2\omega\Gamma(\kappa+1)}{k^3\theta_e^3\kappa^{\frac{3}{2}}\Gamma(\kappa-\frac{1}{2})} + \frac{2\omega_{pb}^2(\omega-kU_b)\Gamma(\kappa+1)}{k^3\theta_b^3\kappa^{\frac{3}{2}}\Gamma(\kappa-\frac{1}{2})} + \frac{2\omega_{pi}^2\omega e^{-\frac{\omega^2}{k^2v_{ti}^2}}}{k^3 v_{ti}^3} + \frac{2\omega_{pp}^2\omega e^{-\frac{\omega^2}{k^2v_{tp}^2}}}{k^3 v_{tp}^3}\right] \quad (5)$$

Here, $\lambda_{Ds} = \sqrt{\frac{T_s\epsilon_0}{n_{0s}e^2z_s^2}} = \frac{v_{ts}}{\omega_{ps}}$ is the Debye length of sth species. The growth/damping rates of electrostatic waves can be obtained as:

$$\gamma = -\frac{D_i}{\frac{\partial D_r}{\partial\omega}}$$

and is given by the following expression

$$\frac{\gamma}{\omega} = -\sqrt{\pi}\left(\frac{\frac{\omega\omega_{pe}^2}{k^3\theta_e^3}\frac{\Gamma(\kappa+1)}{\kappa^{\frac{3}{2}}\Gamma(\kappa-\frac{1}{2})} + \frac{(\omega-kU_b)\omega_{pb}^2}{k^3\theta_b^3}\frac{\Gamma(\kappa+1)}{\kappa^{\frac{3}{2}}\Gamma(\kappa-\frac{1}{2})} + \frac{\omega\omega_{pi}^2 e^{-\frac{\omega^2}{k^2v_{ti}^2}}}{k^3v_{ti}^3} + \frac{\omega\omega_{pp}^2 e^{-\frac{\omega^2}{k^2v_{tp}^2}}}{k^3v_{tp}^3}}{\frac{\omega_{pi}^2}{\omega^2}\left[1+\frac{3k^2v_{ti}^2}{\omega^2}\right] + \frac{\omega_{pp}^2}{\omega^2}\left[1+\frac{3k^2v_{tp}^2}{\omega^2}\right] - \frac{(2\kappa-1)(2\kappa+1)}{(2\kappa-3)^2}\left[\frac{4\omega^2\omega_{pe}^2}{k^4v_{te}^4} + \frac{4\omega(\omega-kU_b)\omega_{pb}^2}{k^4v_{tb}^4}\right]}\right) \quad (6)$$

Real part of dispersion relation, $D_r = 0$ (Eq. (4)) gives the real frequency of electrostatic modes present in the lunar wake plasma and D_i (Eq. 5) imaginary part contains source and damping terms from all the four species considered here. As it stands, this dispersion relation is difficult to analyze analytically. However, if one sets the electron beam density to zero and assume that value of κ is very large (Maxwellian electrons), this equation corresponds to dispersion relation of electrostatic waves in three component plasma, which has a similar form as of ur Rehman et al. (2018, 2019) in the same limits.

An important point that has to be emphasized is this: as one can see from Eq. (4), the dispersion relation hints the existence of six different modes- all of which are acoustic in nature (as acoustic modes, starts at $k = 0$, with $\omega = 0$). This nature is exhibited by all the dispersion curves that we show in the next section. We are only concentrating on the ion acoustic mode as other modes are highly damped. In the next section, Eq. (4) and 6 are analyzed numerically with lunar wake parameters.

3. Numerical analysis

In this section, we analyze Eq. (4) and 6 for plasma parameters relevant to lunar wake. For numerical analysis, we normalize the Eq. (4) and 6 with these set of parameters: all the frequencies by $\omega_{pe} = \sqrt{\frac{N_0e^2}{\epsilon_0 m_e}}$ with $N_0 = n_{0e} + n_{0b} = n_{0p} + z_i n_{0i}$ being total number density of the plasma, wave-number k by $\lambda_{D0} = \sqrt{\frac{\epsilon_0 T_e}{N_0 e^2}}$, velocities by acoustic velocity $c_s = \sqrt{\frac{T_e}{m_p}}$. For numerical computations, plasma parameters are taken from Tao et al. (2012), Mangeney et al. (1999). Table 1 refers to the plasma parameters corresponding to WB1 taken from Tao et al. (2012). It must be noted that the dispersion curves are plotted only in those $k\lambda_{D0}$ range, where the conditions under which plasma dispersion functions have been expanded are satisfied and where positive growth rate is observed. It must be noted that while performing numerical computations, quasi-neutrality condition $n_{0e} + n_{0b} = n_{0p} + z_i n_{0i}$ is always satisfied. Effects of variation of different plasma parameters on electrostatic waves are presented in the next subsections.

3.1. Variation of kappa electron beam velocity

Firstly, we undertake a numerical analysis to study the effects of velocity of kappa electron beam on the electrostatic ion acoustic waves. The normalized parameters fixed for this set of variations are $\frac{n_{0b}}{N_0} = 0.01$, $\frac{n_{0e}}{N_0} = 0.99$, $\frac{n_{0i}}{N_0} = 0.05$, $\frac{n_{0p}}{N_0} = 0.9$, $\frac{T_p}{T_e} = 0.2$, $\frac{T_i}{T_e} = 0.3$, $\frac{T_b}{T_e} = 0.006$ and $\kappa = 6$ (Fig. 2). These parameters are used in subsequent figures as well, unless otherwise studying the effect of variation of particular physical parameter on the wave characteristics. When the beam velocity is set to zero, all the modes are damped as expected due to Landau damping as there is no free energy source to excite the instabilities. It is seen that for given set of parameters, the onset of the positive

Table 1
Plasma parameters from WB1 of Tao et al. (2012).

Plasma parameters	WB1 (From Tao et al. (2012))
Number density (N_0 in cm^{-3})	0.13
Background electron temperature (in eV)	28
Debye length (in m)	108
Super thermality index, κ	6

growth rate occurs at $\frac{U_b}{c_s} = 2.8$. As the velocity of electron beam increases, the growth rate increases and the $k\lambda_{D0}$ range in which the mode becomes unstable increases until $\frac{U_b}{c_s} = 3.8$. Thereafter, $k\lambda_{D0}$ range for unstable plasma waves starts to decrease and assumptions made to expand the plasma dispersion function breaks down beyond $\frac{U_b}{c_s} > 4.3$. As the electron beam velocity $\frac{U_b}{c_s}$ increases, it can be seen from upper panel that the range of real frequencies first tends to increase and then decreases. Also, at fixed value of $k\lambda_{D0}$, the phase speed of the wave increases with increase in electron beam velocity, however, it is smaller than the electron beam velocity. Thus, wave extracts free energy from the beam electrons and grows. Further, for a fixed $k\lambda_{D0}$ value, the real frequency and growth rate increases with increase in electron beam velocity. Since, the real frequency increases, the damping arising due to kappa background electrons (first term in Eq. 6) increases with increase in electron beam velocity whereas damping arising from protons and ions (third and fourth term in numerator of Eq. 6) decreases significantly. In terms of magnitude, the damping arising from proton is largest and helium ions is smallest.

3.2. Variation of superthermality index, κ

In this section, we analyze the effect of superthermality index on dispersion characteristics of electrostatic waves. The parameters fixed for this set of variations are $\frac{u_b}{c_s} = 3$, $\frac{n_{0b}}{N_0} = 0.01$, $\frac{n_{0e}}{N_0} = 0.99$, $\frac{n_{0i}}{N_0} = 0.05$, $\frac{n_{0p}}{N_0} = 0.9$, $\frac{T_p}{T_e} = 0.2$, $\frac{T_i}{T_e} = 0.3$ and $\frac{T_b}{T_e} = 0.006$ (Fig. 3). It is seen that superthermal electron beam favours the growth of the electrostatic ion acoustic waves whereas Maxwellian (larger κ) electron beam suppresses the growth rate. Here, electron beam term (second term in numerator of Eq. 6) play important role. With increase in κ, the contribution of electron beam starts decreasing (becoming less negative) and as system moves towards Maxwellian electron beam the growth rate decreases. This can be corroborated with the fact that there are enough energetic particles/free energy available in superthermal particle distributions to drive these waves unstable. Further, when one takes the value of κ to be high, which corresponds to Maxwell–Boltzmann distribution, Landau damping dominates and wave ceases to grow. The damping rates are higher for protons than the background electrons and helium ions. From Fig. 3, one can see that real frequency is not affected significantly by the change in superthermality index. Wave number range in

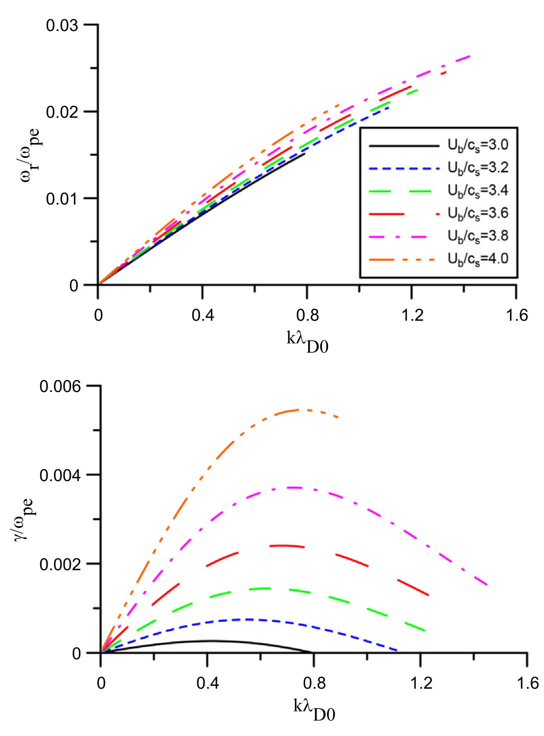

Fig. 2. Dispersion characteristics of ion acoustic waves with different values of kappa electron beam velocity, $\frac{U_b}{c_s}$. Upper and lower panels show the real frequencies and growth rates, respectively. The fixed parameters are $\frac{n_{0b}}{N_0} = 0.01$, $\frac{n_{0e}}{N_0} = 0.99$, $\frac{n_{0i}}{N_0} = 0.05$, $\frac{n_{0p}}{N_0} = 0.9$, $\frac{T_p}{T_e} = 0.2$, $\frac{T_i}{T_e} = 0.3$, $\frac{T_b}{T_e} = 0.006$ and $\kappa = 6$.

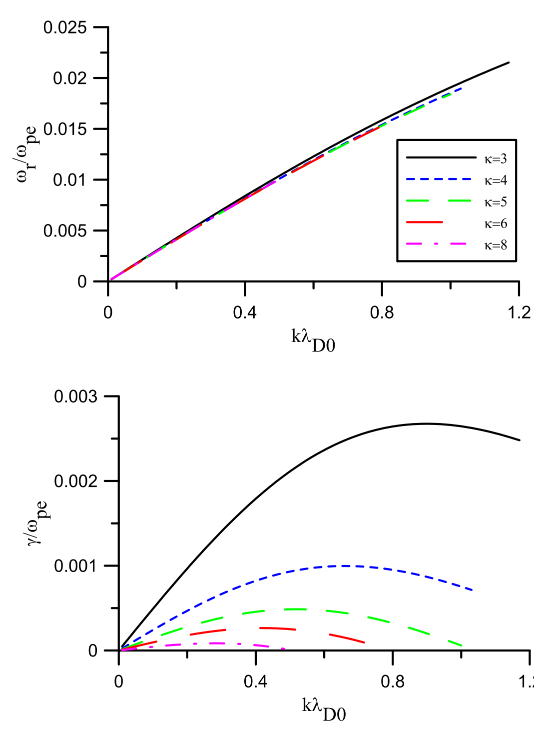

Fig. 3. Dispersion characteristics of ion acoustic waves with different values of superthermality index, κ. Upper and lower panels show the real frequencies and growth rates, respectively. The fixed parameters are $\frac{u_b}{c_s} = 3$, $\frac{n_{0b}}{N_0} = 0.01$, $\frac{n_{0e}}{N_0} = 0.99$, $\frac{n_{0i}}{N_0} = 0.05$, $\frac{n_{0p}}{N_0} = 0.9$, $\frac{T_p}{T_e} = 0.2$, $\frac{T_i}{T_e} = 0.3$ and $\frac{T_b}{T_e} = 0.006$.

which the acoustic mode becomes unstable shrinks with decrease in superthermality.

3.3. Variation of number density of beam electrons

In order to show effect of number density of beam electron on dispersion plots and instability, Eq. (4) and Eq. 6 are analyzed for different number density of electron beam (Fig. 4). The parameters fixed for this variations are $\frac{u_b}{c_s}=3,\ \kappa=6,\ \frac{n_{0i}}{N_0}=0.05,\ \frac{n_{0p}}{N_0}=0.9,\ \frac{T_p}{T_e}=0.2,\ \frac{T_i}{T_e}=0.3$ and $\frac{T_b}{T_e}=0.006$. It is seen that as the beam electrons number density increases, growth rate increases. Furthermore, the phase velocity of ion acoustic waves slightly decreases with increase in electron beam number density. Physically, one can understand this in following way: as the number density of high energetic beam electrons increases, the wave can take much more energy from it. In this scenario, the damping due to background electrons decreases whereas contribution from the beam electrons increases (more negative) with increase in the number density. As the phase velocity of the waves decreases (as shown in Fig. 4), the proton and Helium terms (third and fourth term in Eq. 6) increases. Numerical results show that the damping arising out of background electrons and helium ions are comparable whereas largest damping occurs due to protons. It is also seen that $k\lambda_{D0}$ range first increases and then decreases with increase in number density of beam electrons. The curves have been restricted up to $k\lambda_{D0}$ values where the assumptions on the arguments of the plasma dispersion functions are satisfied.

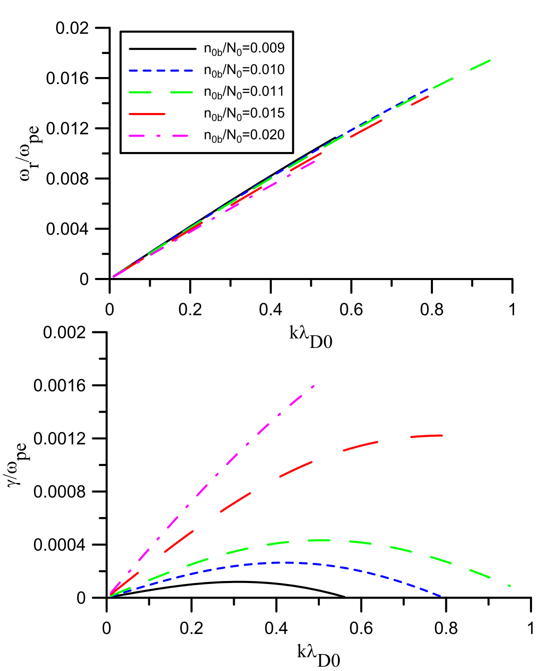

Fig. 4. Dispersion characteristics of ion acoustic waves with different values of kappa electron beam density, $\frac{n_{b0}}{N_0}$. Upper and lower panels show the real frequencies and growth rates, respectively. The fixed parameters are $\frac{u_b}{c_s}=3,\ \frac{n_{0i}}{N_0}=0.05,\ \frac{n_{0p}}{N_0}=0.9,\ \frac{T_p}{T_e}=0.2,\ \frac{T_i}{T_e}=0.3,\ \frac{T_b}{T_e}=0.006$ and $\kappa=6$.

3.4. Variation of number density of doubly charged Helium ions

In this section, we investigate the effect of number density of ions on the electrostatic ion acoustic waves and it is depicted in Fig. 5. The fixed plasma parameters are: $\frac{u_b}{c_s}=3,\ \kappa=6,\ \frac{n_{0b}}{N_0}=0.01,\ \frac{n_{0e}}{N_0}=0.99,\ \frac{T_p}{T_e}=0.2,\ \frac{T_i}{T_e}=0.3$ and $\frac{T_b}{T_e}=0.006$. It is seen that with an increase in the number density of ions, the phase speed of the waves slightly decreases and growth rate increases. The contributions of the proton and Helium damping terms in numerator of Eq. 6 decreases and increases, respectively. Whereas, contributions from background electrons and beam electrons numerator of Eq. 6 decreases and increases, respectively. It is seen that the cumulative effect of all these is to increase the growth rate of the electrostatic ion acoustic waves. For $\frac{n_{i0}}{N_0}>0.2$, our assumptions break down and hence these cases are not shown. The $k\lambda_{D0}$ range for unstable wave increases for $\frac{n_{i0}}{N_0}\leqslant 0.09$ and then starts decreasing. Further, the $k\lambda_{D0}$ value at which maximum growth rate occurs shifts towards higher wave numbers with increase in number density of ions.

3.5. Variation of temperature of protons

The effect of temperature of protons on the characteristics of ion acoustic waves is described in this section and plotted in Fig. 6 with plasma parameters $\frac{u_b}{c_s}=3,\ \kappa=6,\ \frac{n_{0b}}{N_0}=0.01,\ \frac{n_{0e}}{N_0}=0.99,\ \frac{n_{0i}}{N_0}=0.05,\ \frac{n_{0p}}{N_0}=0.9,\ \frac{T_i}{T_e}=0.3$ and

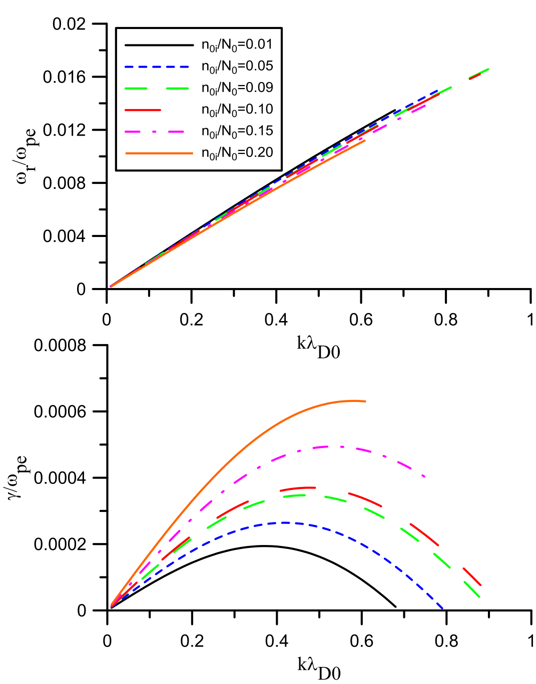

Fig. 5. Dispersion characteristics of ion acoustic waves with different values doubly charged helium ion number density, $\frac{n_{i0}}{N_0}$. Upper and lower panels show the real frequencies and growth rates, respectively. The fixed parameters are $\frac{u_b}{c_s}=3,\ \frac{n_{0b}}{N_0}=0.01,\ \frac{n_{0e}}{N_0}=0.99,\ \frac{T_p}{T_e}=0.2,\ \frac{T_i}{T_e}=0.3,\ \frac{T_b}{T_e}=0.006$ and $\kappa=6$.

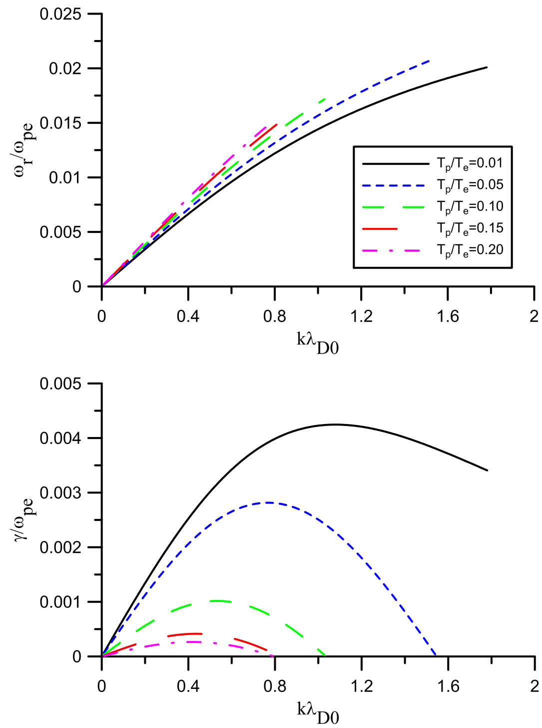

Fig. 6. Dispersion characteristics of ion acoustic waves with different values of temperature of protons, $\frac{T_p}{T_e}$. Upper and lower panels show the real frequencies and growth rates, respectively. The fixed plasma parameters are $\frac{u_b}{c_s}=3$, $\frac{n_{0b}}{N_0}=0.01$, $\frac{n_{0e}}{N_0}=0.99$, $\frac{n_{0i}}{N_0}=0.05$, $\frac{n_{0p}}{N_0}=0.9$, $\frac{T_i}{T_e}=0.3$, $\frac{T_b}{T_e}=0.006$ and $\kappa=6$.

$\frac{T_b}{T_e}=0.006$. It is seen that as the temperature of protons increases, the growth rate decreases. Here, both background electron and proton terms (first and last term in numerator of Eq. 6) increases, whereas the other two terms decreases. The range of unstable wave numbers ($k\lambda_{D0}$) decreases with increase in T_p/T_e values. This is justified as proton temperature approaches electron temperature Landau damping will be larger and hence ion-acoustic waves will stabilize.

3.6. Variation of temperature of doubly charged Helium ions

The effect of temperature of ions on the instability is shown in Fig. 7 for the fixed plasma parameters; $\frac{u_b}{c_s}=3$, $\kappa=6$, $\frac{n_{0b}}{N_0}=0.01$, $\frac{n_{0e}}{N_0}=0.99$, $\frac{n_{0i}}{N_0}=0.05$, $\frac{n_{0p}}{N_0}=0.9$, $\frac{T_p}{T_e}=0.2$ and $\frac{T_b}{T_e}=0.006$. It is interesting to note real frequency of the ion acoustic waves is not affected by the increase in temperature of doubly charged helium ions. On the other hand, growth rate of ion acoustic waves increases for $\frac{T_i}{T_e}$=0.01–0.1, thereafter it starts to decrease. The unstable wave numbers ($k\lambda_{D0}$) follow the growth rate pattern, i.e., unstable wave numbers range increases for $\frac{T_i}{T_e}$=0.01–0.1 and decreases subsequently.

3.7. Variation of temperature of beam electrons

Fig. 8 shows the effects of temperature of beam electrons on the normalized frequencies and normalized growth rates

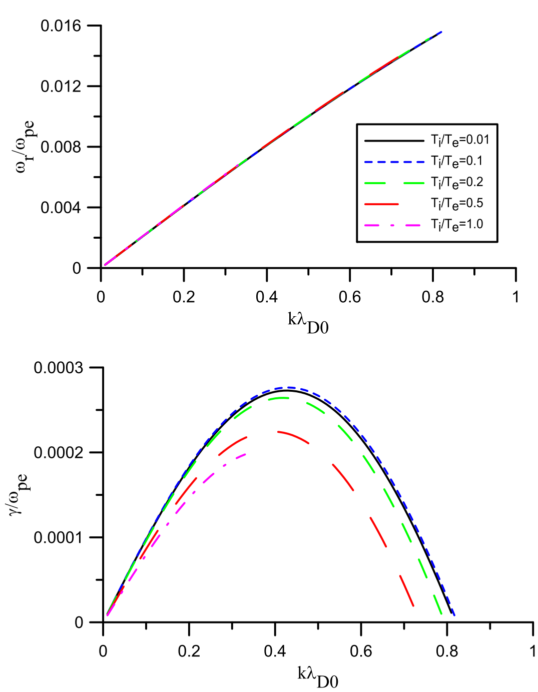

Fig. 7. Dispersion characteristics of ion acoustic waves with different values of ion temperature, $\frac{T_i}{T_e}$,. Upper and lower panels show the real frequencies and growth rates, respectively. The fixed parameters are $\frac{u_b}{c_s}=3$, $\frac{n_{0b}}{N_0}=0.01$, $\frac{n_{0e}}{N_0}=0.99$, $\frac{n_{0i}}{N_0}=0.05$, $\frac{n_{0p}}{N_0}=0.9$, $\frac{T_p}{T_e}=0.2$, $\frac{T_b}{T_e}=0.006$ and $\kappa=6$.

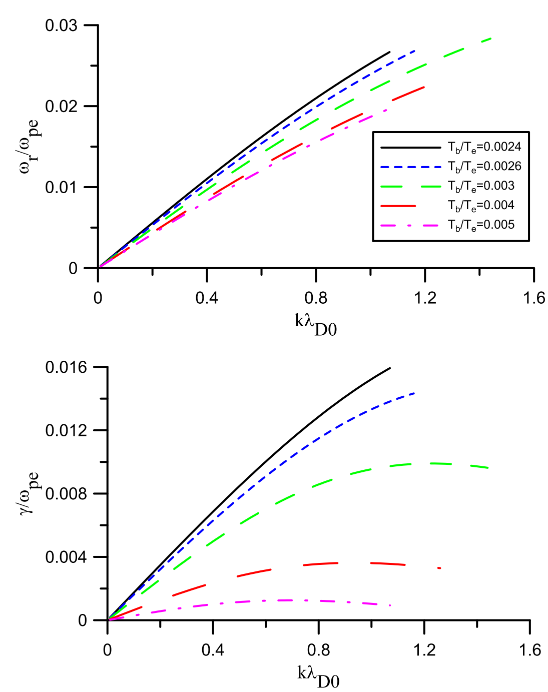

Fig. 8. Dispersion characteristics of ion acoustic waves with different values of electron beam temperature, $\frac{T_b}{T_e}$. Upper and lower panels show the real frequencies and growth rates, respectively. The fixed plasma parameters are $\frac{u_b}{c_s}=3$, $\frac{n_{0b}}{N_0}=0.01$, $\frac{n_{0e}}{N_0}=0.99$, $\frac{n_{0i}}{N_0}=0.05$, $\frac{n_{0p}}{N_0}=0.9$, $\frac{T_p}{T_e}=0.2$, $\frac{T_i}{T_e}=0.3$ and $\kappa=6$.

of ion acoustic waves for the plasma parameters of Fig. 1. It is observed that for small value of $\frac{T_b}{T_e}$, the growth rate is found to be maximum. However, as the value of $\frac{T_b}{T_e}$ increases the growth rate decreases and waves quickly stabilizes. The $k\lambda_{D0}$ range first increases and then decreases with increase in $\frac{T_b}{T_e}$. It is seen that background electron contribution in numerator of Eq. 6 decreases with increase in temperature of beam electrons, however, the kappa-beam term, proton term and Helium term in numerator of Eq. 6 increases.

4. Discussions and conclusions

We have investigated the effect of various plasma parameters on the frequency and growth rate of ion acoustic waves in lunar wake plasma modelled by background and beam electrons having kappa distributions, and Maxwell–Boltzmann distributed protons and doubly charged Helium ions. The previous studies (Sreeraj et al., 2018; Sreeraj et al., 2020), had concentrated on non-resonant instability employing fluid theory. In this paper, we have used kinetic theory to study the excitation of ion-acoustic waves driven by a resonant instability. It is seen that the ion acoustic waves are excited by the electron beam. Onset of instability for the electrostatic mode happens at lower beam velcoity than compared with those seen in Sreeraj et al. (2018). It is found that increase in the electron beam velocity and number density of both beam electron and double charged Helium ions enhance the growth rate of ion acoustic waves, whereas increase in kappa value, temperature of protons and temperature of beam electrons reduce the growth rate. For the lunar wake plasma parameters, maximum damping comes from the protons whereas damping from background electrons and helium ions are comparable. The growth rates and wavelengths of the excited ion acoustic waves here are larger and smaller, respectively as compared to the magnetized and unmagnetized cases considered in Sreeraj et al. (2018, 2020). Further, excited ion acoustic waves have frequencies much closer to the observed wave frequencies in the burst WB1.

We have delineated the electrostatic wave observed by ARTEMIS P1 satellite on its first flyby of the lunar wake. The two of the three wave bursts namely, WB2 and WB3 which have frequencies in the range of (0.1–0.4) f_{pe} have been explained by kinetic theory of electron beam mode in a Vlasov simulation by Tao et al. (2012). However, frequencies in wave burst WB1 being much lower $f \sim 0.01 f_{pe}$ could not be explained by invoking high-frequency electron beam mode. Since the frequencies are of the order of ion plasma frequencies, we developed a kinetic model to study the low frequency ion-acoustic waves. The numerical results on generation of ion acoustic waves with variation of various plasma parameters have provided us wave frequencies (refer to Figs. 2–8) below $f \simeq 0.03 f_{pe}$. The observed WB1 parameters are: estimated density, $N_0 = 0.13\text{cm}^{-3}, \lambda_{D0} = 108\text{m}$, the corresponding background electron temperature, $T_e = 28\text{eV}$ and electron plasma frequency f_{pe}=3238 Hz, ion acoustic speed, $c_s \approx 52$ km/s. From Fig. 2, it is observed that for $U_b/c_s = 3 - 4$, the wave frequencies are in the range of $f \approx (0.0085 - 0.018) f_{pe}$ corresponding to peak growth rates of $\gamma \approx (0.00026 - 0.00545) f_{pe}$. These peak growth rates occur at $k\lambda_{D0} \approx 0.42 - 0.76$. The phase speed of the electrostatic waves are calculated to be $v_{ph} \sim$(44.5–51.8) km/s and wavelengths are of the order $\sim$ (1615–892) m. The observed ion acoustic speed is $c_s \sim 51.8$ km/s and wave frequencies are as low as $f \simeq 0.01 f_{pe}$, respectively. The observed frequencies are less than the total ion plasma frequency (0.0233f_{pe} in this case). It suggests that observed electrostatic waves are dispersive in nature. Our theoretical model predicts wave phase speeds and wave frequencies less than the ion acoustic speed and ion plasma frequency, respectively. Thus, it signifies the fact that the observed waves are ion-acoustic waves, driven by electron beam and our theoretical prediction matches very well with the low-frequency ($\sim$0.01 f_{pe}) electrostatic waves observed in the lunar wake by Tao et al. (2012). However, in order to excite these low frequency electrostatic waves, one requires low-energy ($\sim$ 0.1 eV) electron beams, which are undetected by ARTEMIS. It would be worthwhile to look for such low-energy electron beams in the ARTEMIS or any other satellite mission's particle data to verify the prediction of our model.

Data availability

The data used in the manuscript is taken from Tao, J. B., Ergun, R. E., Newman, D. L. et al. (2012). Kinetic instabilities in the lunar wake: ARTEMIS observations. Journal of Geophysical Research: Space Physics, 117 (A3), A03106. doi:10.1029/2011ja017364 (Tao et al., 2012) and Mangeney, A., Salem, C., Lacombe, C. et al. (1999). WIND observations of coherent electrostatic waves in the solar wind. Annales Geophysicae, 17(3), 307–320. doi:10.1007/s00585-999–0307-y (Mangeney et al., 1999).

Declaration of Competing Interest

The authors declare that they have no known competing financial interests or personal relationships that could have appeared to influence the work reported in this paper.

Acknowledgments

GSL thanks the Indian National Science Academy, New Delhi for the support under the INSA-Honorary Scientist Scheme.

References

Angelopoulos, V., 2008. The THEMIS mission. Space Sci. Rev. 141 (1–4), 5–34. https://doi.org/10.1007/s11214-008-9336-1.

Backrud, M., Tjulin, A., Vaivads, A., et al., 2005. Interferometric identification of ion acoustic broadband waves in the auroral region:

CLUSTER observations. Geophys. Res. Lett. 32 (21), L21109. https://doi.org/10.1029/2005gl022640.
Bale, S.D., 1997. Shadowed particle distributions near the moon. J. Geophys. Res.: Space Phys. 102 (A9), 19773–19778. https://doi.org/10.1029/97ja01676.
Bale, S.D., Owen, C.J., Bougeret, J.-L., et al., 1997. Evidence of currents and unstable particle distributions in an extended region around the lunar plasma wake. Geophys. Res. Lett. 24 (11), 1427–1430. https://doi.org/10.1029/97gl01193.
Bhardwaj, A., Dhanya, M., Alok, A., et al., 2015. A new view on the solar wind interaction with the moon. Geosci. Lett. 2 (1). https://doi.org/10.1186/s40562-015-0027-y.
Bosqued, J.M., Lormant, N., Rème, H., et al., 1996. Moon-solar wind interactions: First results from the WIND/3dp experiment. Geophys. Res. Lett. 23 (10), 1259–1262. https://doi.org/10.1029/96gl00303.
Chen, H., Yang, W., Liu, S., 2019. Dust-ion-acoustic modes at comet 67p/churyumov-gerasimenko. Phys. Plasmas 26 (11), 112104. https://doi.org/10.1063/1.5124543.
Cully, C.M., Ergun, R.E., Stevens, K., et al., 2008. The THEMIS digital fields board. Space Sci. Rev. 141 (1–4), 343–355. https://doi.org/10.1007/s11214-008-9417-1.
Forslund, D.W., 1970. Instabilities associated with heat conduction in the solar wind and their consequences. J. Geophys. Res. 75 (1), 17–28. https://doi.org/10.1029/ja075i001p00017.
Fried, B.D., 1961. Longitudinal ion oscillations in a hot plasma. Phys. Fluids 4 (1), 139. https://doi.org/10.1063/1.1706174.
Guo, D., Zhang, X., Xie, L., et al., 2019. Diamagnetic plasma clouds in the near lunar wake observed by ARTEMIS. Astrophys. J. 883 (1), 12. https://doi.org/10.3847/1538-4357/ab3652.
Halekas, J.S., 2005. Electrons and magnetic fields in the lunar plasma wake. J. Geophys. Res. 110 (A7), A07222. https://doi.org/10.1029/2004ja010991.
Halekas, J.S., Angelopoulos, V., Sibeck, D.G., et al., 2011. First results from ARTEMIS, a new two-spacecraft lunar mission: Counter-streaming plasma populations in the lunar wake. Space Sci. Rev. 165 (1–4), 93–107. https://doi.org/10.1007/s11214-010-9738-8.
Harada, Y., Halekas, J.S., 2016. Upstream waves and particles at the moon. In: Low-Frequency Waves in Space Plasmas. John Wiley & Sons Inc, pp. 307–322. https://doi.org/10.1002/9781119055006.ch18.
Hess, R.A., MacDowall, R.J., Goldstein, B., et al., 1998. Ion acoustic-like waves observed by ulysses near interplanetary shock waves in the three-dimensional heliosphere. J. Geophys. Res.: Space Phys. 103 (A4), 6531–6541. https://doi.org/10.1029/97ja03395.
Hutchinson, I.H., Malaspina, D.M., 2018. Prediction and observation of electron instabilities and phase space holes concentrated in the lunar plasma wake. Geophys. Res. Lett. 45 (9), 3838–3845. https://doi.org/10.1029/2017gl076880.
Liu, Z., Du, J., 2009. Dust acoustic instability driven by drifting ions and electrons in the dust plasma with lorentzian kappa distribution. Phys. Plasmas 16 (12), 123707. https://doi.org/10.1063/1.3274459.
Livadiotis, G., 2015. Introduction to special section on origins and properties of kappa distributions: Statistical background and properties of kappa distributions in space plasmas. J. Geophys. Res.: Space Phys. 120 (3), 1607–1619. https://doi.org/10.1002/2014ja020825.
Lonngren, K., Montgomery, D., Alexeff, I., et al., 1967. Dispersion of ion-acoustic waves. Phys. Lett. A 25 (8), 629–630. https://doi.org/10.1016/0375-9601(67)90298-8.
Mace, R.L., Hellberg, M.A., 1995. A dispersion function for plasmas containing superthermal particles. Phys. Plasmas 2 (6), 2098–2109. https://doi.org/10.1063/1.871296.
Mangeney, A., Salem, C., Lacombe, C., et al., 1999. WIND observations of coherent electrostatic waves in the solar wind. Ann. Geophys. 17 (3), 307–320. https://doi.org/10.1007/s00585-999-0307-y.
McFadden, J.P., Carlson, C.W., Larson, D., et al., 2008. The THEMIS ESA plasma instrument and in-flight calibration. Space Sci. Rev. 141 (1–4), 277–302. https://doi.org/10.1007/s11214-008-9440-2.
Meng, Z., Thorne, R.M., Summers, D., 1992. Ion-acoustic wave instability driven by drifting electrons in a generalized lorentzian distribution. J. Plasma Phys. 47 (3), 445–464. https://doi.org/10.1017/s002237780002434x.
Nakagawa, T., 2016. ULF/ELF waves in near-moon space. In: Low-Frequency Waves in Space Plasmas. John Wiley & Sons Inc., pp. 293–306. https://doi.org/10.1002/9781119055006.ch17.
Olbert, S., 1968. Summary of experimental results from m.i.t. detector on IMP-1. In: Physics of the Magnetosphere. Springer, Netherlands, pp. 641–659. https://doi.org/10.1007/978-94-010-3467-8_23.
ur Rehman, S., ul Haque, Q., Shah, A., 2018. Interplanetary ion acoustic wave in solar wind plasma. Phys. Plasmas 25(8), 084503. https://doi.org/10.1063/1.5028338.
ur Rehman, S., Shah, A., ul Haque, Q., 2019. Kinetic theory of ion acoustic waves observed at comet 67p/churyumov–gerasimenko. Astrophys. J. 880(1), L13. https://doi.org/10.3847/2041-8213/ab2f8d.
Rubia, R., Singh, S.V., Lakhina, G.S., 2017. Occurrence of electrostatic solitary waves in the lunar wake. J. Geophys. Res.: Space Phys. 122 (9), 9134–9147. https://doi.org/10.1002/2017ja023972.
Scarf, F.L., Coroniti, F.V., Kennel, C.F., et al., 1986. Plasma wave observations at comet giacobini-zinner. Science 232 (4748), 377–381. https://doi.org/10.1126/science.232.4748.377.
Sreeraj, T., Singh, S.V., Lakhina, G.S., 2018. Electrostatic waves driven by electron beam in lunar wake plasma. Phys. Plasmas 25 (5), 052902. https://doi.org/10.1063/1.5032141.
Sreeraj, T., Singh, S.V., Lakhina, G.S., 2020. Linear analysis of electrostatic waves in the lunar wake plasma. Phys. Scr. 95 (4), 045610. https://doi.org/10.1088/1402-4896/ab7142.
Summers, D., Thorne, R.M., 1992. A new tool for analyzing microinstabilities in space plasmas modeled by a generalized lorentzian (kappa) distribution. J. Geophys. Res. 97 (A11), 16827. https://doi.org/10.1029/92ja01664.
Tao, J.B., Ergun, R.E., Newman, D.L., et al., 2012. Kinetic instabilities in the lunar wake: ARTEMIS observations. J. Geophys. Res.: Space Phys. 117 (A3), A03106. https://doi.org/10.1029/2011ja017364.
Vasyliunas, V.M., 1968. A survey of low-energy electrons in the evening sector of the magnetosphere with OGO 1 and OGO 3. J. Geophys. Res. 73 (9), 2839–2884. https://doi.org/10.1029/ja073i009p02839.
Wiehle, S., Plaschke, F., Motschmann, U., et al., 2011. First lunar wake passage of ARTEMIS: Discrimination of wake effects and solar wind fluctuations by 3d hybrid simulations. Planet. Space Sci. 59 (8). https://doi.org/10.1016/j.pss.2011.01.012.
Wong, A.Y., Motley, R.W., D'Angelo, N., 1964. Landau damping of ion acoustic waves in highly ionized plasmas. Phys. Rev. 133 (2A), A436–A442. https://doi.org/10.1103/physrev.133.a436.
Zaheer, S., Murtaza, G., Shah, H.A., 2004. Some electrostatic modes based on non-maxwellian distribution functions. Phys. Plasmas 11 (5), 2246–2255. https://doi.org/10.1063/1.1688330.